








## Green synthesis of iron nanoparticles (Fe(NPs)) using plant extract from *Eucalyptus grandis*: characterization and determination of the catalytic potential for reduction of 4-nitrophenol

ARTICLES doi:10.4136/ambi-agua.2978

Received: 06 Dec. 2023; Accepted: 29 May 2024

Filipe Kalil da Silva Naves<sup>1\*</sup>; Yasmin Milena Loth Bueno<sup>1</sup>  
Raquel Dalla Costa da Rocha<sup>1,2</sup>; Rodrigo Brackmann<sup>1,2</sup>  
Marcio Barreto Rodrigues<sup>1,2</sup>

<sup>1</sup>Programa de Pós-Graduação em Tecnologia de Processos Químicos e Bioquímicos. Universidade Tecnológica Federal do Paraná (UTFPR), Via do Conhecimento, s/n, km 01, CEP: 85503-390, Pato Branco, PR, Brazil.

E-mail: yasmin-milena@hotmail.com, raqueldcr@utfpr.edu.br, marciorodrigues@utfpr.edu.br

<sup>2</sup>Departamento de Química. Universidade Tecnológica Federal do Paraná (UTFPR),

Via do Conhecimento, s/n, KM 01, CEP: 85503-390, Pato Branco, PR, Brazil.

E-mail: raqueldcr@utfpr.edu.br, rodrigobrackmann@utfpr.edu.br, marciorodrigues@utfpr.edu.br

\*Corresponding author. E-mail: filipenaves@alunos.utfpr.edu.br

### ABSTRACT

This study assessed a green synthesis method for iron nanoparticles (Fe(NPs)), using *Eucalyptus grandis* leaf extract, to reduce waste generation and diminish the use of conventional chemical inputs, such as Sodium Borohydride (NaBH<sub>4</sub>), without significant losses in catalytic activity. Various volumetric ratios of plant extract and NaBH<sub>4</sub> were tested to understand how this variation would affect the morphological, structural, and catalytic power of the material. In the conducted analyses, a reduction in the crystallinity of Fe(NPs) was observed for proportions above 25% of the extract. However, the particle size remained stable among different syntheses, with iron ions showing improved dispersion for proportions of 40% and 50% of the extract. Regarding stabilization, characteristic bands of aromatic compounds, alcohols, ethers and carboxylic acids were identified, indicating the extract's involvement in coating the metallic cores. To assess the catalytic performance, studies were conducted on the catalytic reduction of the contaminant 4-nitrophenol to 4-aminophenol, using Fe(NPs) as catalysts. The results revealed conversions above 80% for Fe(NPs) synthesized with volumetric proportions of up to 40% of the plant extract, suggesting that substituting the chemical agent did not significantly affect the catalytic activity of the biocatalyst. Finally, ecotoxicological tests performed with *Lemna minor* and *artemia salina* demonstrated a significant reduction in the toxicity of the contaminant 4-nitrophenol, as well as the biocompatibility of the obtained Fe(NPs).

**Keywords:** iron oxides, stabilization, vegetable coating.



# Síntese verde de nanopartículas de ferro (Fe(NPs)) empregando extrato vegetal de *Eucalyptus grandis*: caracterização e determinação do potencial catalítico para redução de 4-nitrofenol acronyms

## RESUMO

O objetivo deste estudo foi avaliar um método de síntese verde de nanopartículas de ferro (Fe(NPs)) utilizando o extrato das folhas de *Eucalyptus grandis*, visando reduzir a geração de resíduos e diminuir o uso de insumos químicos convencionais, como o Borohidreto de sódio ( $\text{NaBH}_4$ ), sem comprometer a atividade catalítica. Diversas proporções volumétricas do extrato vegetal e de agente redutor  $\text{NaBH}_4$  foram testadas para compreender como essa variação afetaria as características morfológicas, estruturais e o poder catalítico do material. Nas análises realizadas, observou-se uma redução na cristalinidade das Fe(NPs) para proporções acima de 25% do extrato. No entanto, o tamanho das partículas permaneceu estável entre as diferentes sínteses, destacando-se o fato de que os íons de ferro apresentaram melhor dispersão em proporções de 40% e 50% do extrato. Em relação à estabilização, foram identificadas bandas características de compostos fenólicos, álcoois e ácidos carboxílicos, evidenciando a atuação do extrato no revestimento dos núcleos metálicos. Para avaliar o desempenho catalítico, foram conduzidos estudos de redução catalítica do contaminante 4-nitrofenol a 4-aminofenol, utilizando as Fe(NPs) como catalisadores. Os resultados revelaram conversões acima de 80% para as Fe(NPs) sintetizadas com proporções volumétricas de até 40% do extrato vegetal, indicando que a substituição do agente químico não afetou significativamente a atividade catalítica do biocatalisador. Por fim, os testes ecotoxicológicos realizados com *Lemna minor* e artemia salina demonstraram uma redução significativa na toxicidade do contaminante 4-nitrofenol, além de comprovar a biocompatibilidade das Fe(NPs) obtidas.

**Palavras-chave:** estabilização, óxidos de ferro, revestimento vegetal.

## 1. INTRODUCTION

The term "Nano" is a prefix denoting physical dimensions corresponding to one billionth of a meter ( $10^{-9}$  m). Due to these dimensions, nanotechnology has revolutionized the conceptual world, enabling the manipulation of structures at extremely reduced scales, thus exploring intrinsic properties such as geometry, atomic structure, conductivity, and magnetism, thereby highlighting the individual characteristics of particles (Bhole *et al.*, 2023). These characteristics, which underscore its enormous potential, have led to the application of nanotechnology in various fields such as materials engineering, nanomedicine, microfluidics, electronics, energy, and the environment (Vinayagam *et al.*, 2024).

Nanoparticles have assumed an innovative perspective with the advent of nanotechnology knowledge, particularly when individual particle monitoring became possible. Nanoscale particles exhibit specific properties due to their proximity to atomic-molecular dimensions, involving phenomena and concepts from both quantum and classical physics (Chung *et al.*, 2016). In this context, iron nanoparticles (Fe(NPs)) exhibit excellent characteristics, such as high catalytic properties, optimal adsorption capacity, reactivity, mechanical properties, biocompatibility, and chemical and thermal stability, which stimulate research in search of new applications and functionalities (Sridevi *et al.*, 2023).

However, a negative factor in the synthesis of Fe(NPs), which often hinders industrial-scale processes, is the toxicity of the reagents used in the procedures. For example, techniques such as microemulsion (Salvador *et al.*, 2021), chemical co-precipitation (Ke *et al.*, 2011), and pulse electrodeposition (Mohanty, 2011), commonly used in nanoparticle synthesis, involve the use of compounds such as benzene ( $\text{C}_6\text{H}_6$ ), ammonia ( $\text{NH}_3$ ), and boric acid ( $\text{H}_3\text{BO}_3$ ),

respectively. The presence of these chemical substances in synthesis processes can result in the generation of residues that have the potential to cause harmful impacts on the environment at various trophic levels. It is important to note that exposure to these chemical substances can not only directly affect organisms present in ecosystems but also cause cascading adverse effects, influencing population dynamics and the structure of natural habitats (Santos *et al.*, 2022).

In light of this scenario, alternative synthesis methods have gained prominence in recent decades. These methods stem from the concepts of green chemistry, which aim to develop chemical processes minimizing environmental impact, promoting sustainability. More specifically, green synthesis is distinguished by employing natural reducing agents, more efficient and environmentally clean energy sources, and renewable raw materials, among other characteristics (Naikoo *et al.*, 2021), thus representing a significant approach aligned with the sustainability principles established by the United Nations (UN) in September 2017.

In this context, aiming at minimizing environmental impacts and promoting sustainability, the present study conducted green synthesis of Fe(NPs) using different volumetric ratios of aqueous extract from the leaves of *Eucalyptus grandis* and sodium borohydride ( $\text{NaBH}_4$ ), evaluating to what extent the chemical agent can be replaced by the extract without compromising the physicochemical properties and catalytic activity of the nanomaterials.

*Eucalyptus* extracts are employed in green synthesis of nanoparticles due to the presence of various secondary metabolites and bioactive components, such as polyphenols, flavonoids, organic acids, amino acids, terpenes, reducing sugars, vitamins, among others (Maikudi *et al.*, 2021). These components play essential roles in reducing metallic ions and stabilizing nanoparticles, minimizing agglomeration formation. Various parts of plants (such as leaves, roots, stems, fruits, seeds, etc.) can be employed in this type of synthesis, as long as they have the capacity to act as reducing and stabilizing agents (Khairul and Sapawe, 2020). Therefore, the Ferric Reducing Antioxidant Power (FRAP) methodology was employed to evaluate the reducing potential of *Eucalyptus* plant extract on iron, and various instrumental techniques were used to assess the structural, physicochemical properties, and the potential coating of the plant extract on Fe(NPs), aiding in their stabilization.

Figure 1 displays the schematic diagram of the main developed stages.

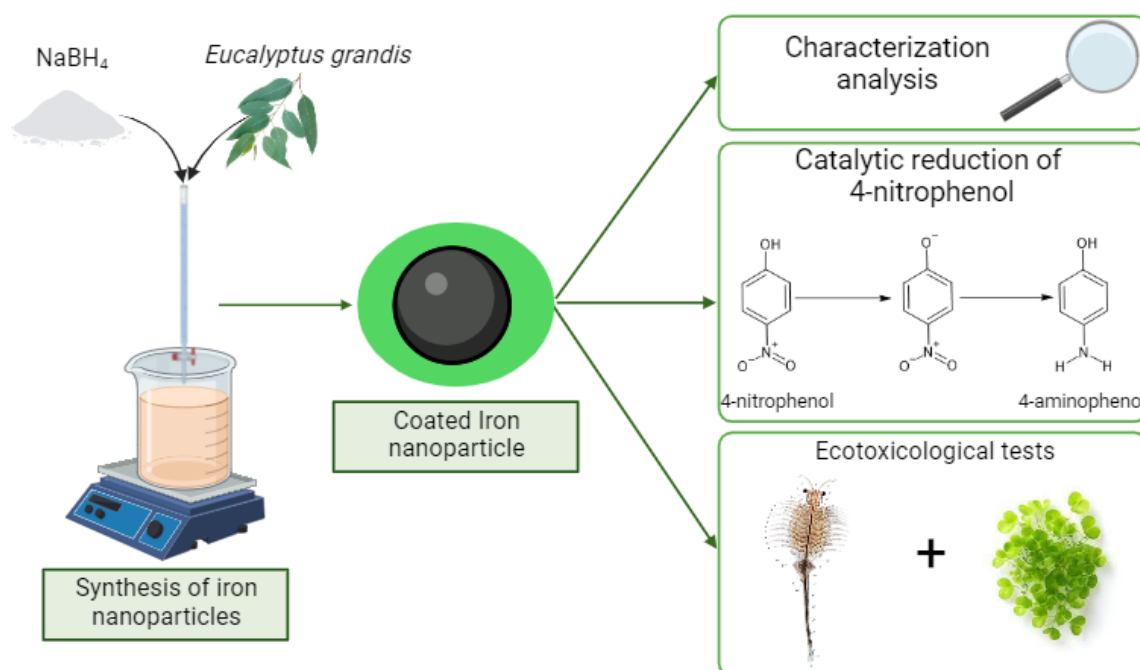


**Figure 1.** Schematic diagram of the main developed stages.

## 2. METHODOLOGY

### 2.1. Aqueous extract of *Eucalyptus* leaves

Extraction was performed according to the procedure described by Samari and collaborators with modifications (Samari *et al.*, 2018). The leaves of *Eucalyptus grandis* were collected in the city of Votuporanga-SP (Brazil) in the summer, then washed with distilled water to remove impurities, dried at room temperature in the shade for seven days (to avoid loss of volatile compounds), and crushed to obtain a powder of organic material. With this, 10 g of leaf powder was added to an Erlenmeyer flask along with 100 mL of distilled water. The mixture remained under constant stirring and was heated at 80°C for 10 min on a magnetic stirrer. Furthermore, the aqueous extract was filtered with Whatman n° 1 filter paper and subsequently used in the synthesis of Fe(NPs).

The extract underwent the Ferric Reducing Antioxidant Power (FRAP) assay, as described by Benzie and Strain (1996) and replicated by Dudonné and collaborators (2009) for the eucalyptus extract (Dudonné *et al.*, 2009), to assess its reduction potential. For this purpose, 100  $\mu\text{L}$  of the aqueous extract was combined with 3 mL of the FRAP reagent, which was composed of 25 mL of 0.3 mol L<sup>-1</sup> acetate buffer, 2.5 mL of 10 mmol L<sup>-1</sup> TPTZ (2,4,6-tris(2-pyridyl)-5-triazine) solution, and 2.5 mL of 20 mmol L<sup>-1</sup> aqueous ferric chloride (FeCl<sub>3</sub>) solution. Subsequently, the mixture was vortexed to achieve homogeneity and incubated in a water bath at 37°C for 30 minutes, shielded from light. The absorbance was then measured using a UV-VIS spectrophotometer at 595 nm, with zeroing performed using the FRAP reagent. To quantify the results, a standard curve of ferrous sulfate (FeSO<sub>4</sub>) was constructed ranging from 200 to 2000  $\mu\text{mol g}^{-1}$ . The results obtained from the FRAP analysis serve as a tool for evaluating the effectiveness of the extraction process in obtaining an extract with high reducing potential. This assessment determines the capacity of the aqueous extract to participate in the stage of reduction of Fe(NPs).

### 2.2. Green synthesis of Fe(NPs) with different volumetric proportions of plant extract and NaBH<sub>4</sub>

In this step, initially, the iron precursor solution was prepared, formed by solutions of 0.05 mol L<sup>-1</sup> of iron chloride hexahydrate (FeCl<sub>3</sub>·6H<sub>2</sub>O) and 0.05 mol L<sup>-1</sup> of iron sulfate heptahydrate (FeSO<sub>4</sub>·7H<sub>2</sub>O) in a 1:1 ratio. Then, the precursor solution was added to a beaker and a titration system was prepared on this beaker with an approximate rate of 0.5 mL s<sup>-1</sup>, which was first used to add the 0.2 mol L<sup>-1</sup> solution of (NaBH<sub>4</sub>), and 5 minutes after the end of the NaBH<sub>4</sub> drip, used to add the plant extract. During the entire synthesis process, the mixture remained under stirring at 400 rpm on a magnetic stirrer and the beaker was sealed with film paper to prevent further interaction with atmospheric gases. The mixture remained under stirring for 30 min after the end of NaBH<sub>4</sub> dripping. Therefore, the Fe(NPs) were vacuum filtered and washed with distilled water, and then stored in a Drybox.

In this synthesis, four Fe(NPs) were prepared, in which the iron precursor solution was responsible for 50% of the total volume, that is, 250 mL. The first was composed of 50% (250 mL) of NaBH<sub>4</sub> and 0 mL of plant extract (Fe(NPs) 0%). The second was formed with 25% (125 mL) of NaBH<sub>4</sub> and 25% (125 mL) of the extract (Fe(NPs)-E 25%). The third was composed of 10% (50 mL) of NaBH<sub>4</sub> and 40% (200 mL) of the aqueous extract (Fe(NPs)-E 40%). Finally, the fourth Fe(NPs) was formed only with the extract, that is, 50% (250 mL) of the plant extract (Fe(NPs)-E 50%). The mixing proportions of the reagents have been detailed in Table 1.

**Table 1.** Volumetric proportions/percentages of the initial mixture in the reaction medium.

Nanoparticle	Iron precursor solution	NaBH <sub>4</sub>	Eucalyptus Extract
Fe(NPs) 0%	50% (250 mL)	50% (250 mL)	0% (0 mL)
Fe(NPs)-E 25%	50% (250 mL)	25% (125mL)	25% (125mL)
Fe(NPs)-E 40%	50% (250 mL)	10% (50 mL)	40% (200 mL)
Fe(NPs)-E 50%	50% (250 mL)	0% (0 mL)	50% (250 mL)

### 2.3. Characterizations of Fe(NPs)

To evaluate the composition of Fe(NPs), X-ray diffractometry (XRD) was used, comparing the material with the database. In this analysis, a Miniflex 600 Model equipment (Rigaku) was used, with a scanning range of 10-90°, in step mode, with a step of 0.02° and a step time of 2 s. To evaluate the plant coating, spectroscopy in the infrared region with Fourier transform (FTIR) was employed on the Frontier equipment, Perkin Elmer® (USA). In FTIR, the Attenuated Total Reflectance (ATR) mode was employed, with a spectral range of 400-4000 cm<sup>-1</sup>, with a number of accumulations of 32 scans and a resolution of 4 cm<sup>-1</sup>. Thermogravimetric analysis (TG-DTA) was employed on Model SDT Q600 equipment (TA instruments), at a synthetic air atmosphere with a flow of 50 mL min<sup>-1</sup>, with the temperature varying from 25 to 1000°C with a heating rate of 10°C min<sup>-1</sup>. To evaluate the morphology of the samples, scanning electron microscopy (SEM) using Tescan equipment, Model Vega3 with Quorum metallizer, model SC7620, which is coupled to an energy dispersive spectroscopy detector (EDS) Oxford, Model x-Act, and High-performance field emission scanning electron microscopy (HR-FESEM) on a Tescan equipment, Model Mira3 were employed.

The BET (Brunauer-Emmett-Teller) analysis was conducted using the Quantachrome NOVA automated gas sorption system, employing N<sub>2</sub> adsorption at -196°C for 6 hours, with relative pressure (P/P<sub>0</sub>) ranging from 0.002 to 0.95.

### 2.4. Catalytic reduction of 4-nitrophenol to 4-aminophenol

The analysis was used to evaluate the catalytic potential of the Fe(NPs), observing whether the different compositions influence the catalytic performance, employing the methodology described by Sravanthi *et al.* (2019), with modifications. During the analysis, 4 mL aliquots were removed at 2 min time intervals and evaluated using molecular absorption spectroscopy (UV-Vis) at a wavelength of 400 nm. For this, 100 mL of an aqueous solution of 4-nitrophenol (10 mg L<sup>-1</sup>) was mixed with 40 mg of Fe(NPs). Next, a vigorous stirring ensued for 2 minutes using a magnetic stirrer. Subsequently, 50 mL of an 0.2 mol L<sup>-1</sup> NaBH<sub>4</sub> aqueous solution was added to the mixture. This compound acts as a reducing agent in the process and in the alkalization of the reaction medium, converting 4-nitrophenol to 4-nitrophenolate, which is more susceptible to catalytic reduction. Then, stirring continued until the solution turned colorless. During the entire process, the temperature remained constant at 50°C. Throughout the process, the conversion of 4-nitrophenol to 4-nitrophenolate takes place by the addition of NaBH<sub>4</sub>, causing its maximum absorption peak to shift from 360 to 400 nm. Subsequently, the reduction in signal intensity at 400 nm is assessed, indicating the conversion of 4-nitrophenolate to 4-aminophenol (Sravanthi *et al.*, 2019).



## 2.5. Ecotoxicological tests

At this stage, ecotoxicological tests were carried out on the trophic levels of microcrustaceans (*Artemia salina*) and aquatic plants (*Lemna minor*). The objectives were first to evaluate whether there is a reduction in the toxicity of 4-nitrophenol after catalytic reduction, comparing it with 4-nitrophenol before the test; for this, the last aliquot taken from a reduction test was used. Furthermore, the tests were employed to evaluate the toxicity of Fe(NPs) leachates and of NaBH<sub>4</sub>.

The first ecotoxicological test took place on the trophic level of microcrustaceans. Initially, in this acute test, the glassware is cleaned with water, detergent and alcohol 70. With this, Meyer's medium (culture medium) is prepared by adding: 0.7 g of potassium chloride (KCl), 1.3 g of calcium chloride (CaCl<sub>2</sub>), 23 g of sodium chloride (NaCl), 11 g of magnesium chloride hexahydrate (MgCl<sub>2</sub>.6H<sub>2</sub>O) and 4 g of sodium sulfate (Na<sub>2</sub>SO<sub>4</sub>) in one liter of distilled water, adjusting the pH to 9 for the culture medium. The blank (BR) was formed only by Meyer's medium. For this test, it was necessary to adjust pH to 9 for all samples, considering that this is the pH at which microcrustaceans are normally found. Furthermore, for the hatching process, the cysts were added to the culture medium for 48 hours, at 28°C, under continuous light and oxygenation. After hatching, 10 nauplii were added to each culture well along with 10 mL of the sample to be tested. Therefore, the culture wells were re-subjected to continuous light at 28°C for 24 to 48 hours. Then, the dead and/or immobilized microcrustaceans were counted. In this analysis 4-nitrophenol (10 mg L<sup>-1</sup>) before catalytic reduction, the last aliquot taken from the catalytic reduction with Fe(NPs)-E 40%, NaBH<sub>4</sub> and the leachates of Fe(NPs)-E 25% and Fe(NPs) 0% were tested.

The second ecotoxicological test took place on the trophic level of aquatic plants. Initially, it was necessary to sanitize the glassware with water, detergent and alcohol 70. Therefore, the next step was to adjust the pH to 7.5 for all samples, and then 10 mL of the samples to be tested and 10 fronds were added to the wells. Finally, the wells were subjected to continuous light at 18 to 22°C for 7 days. After 7 days, the cloning analysis takes place. In this test 4-nitrophenol before catalytic reduction (10 mg L<sup>-1</sup>), the last aliquot taken from catalytic reduction with Fe(NPs)-E 50%, NaBH<sub>4</sub> and the leachates of Fe(NPs)-E 25% and Fe(NPs) 0% were tested.

## 3. RESULTS AND DISCUSSION

### 3.1. FRAP and XRD

In the FRAP analysis, the extract had to be initially diluted 100 times to bring it within the range of the standard curve values. Subsequently, a value of 133.72 mmol g<sup>-1</sup> was obtained. Therefore, the extract has a good reducing capacity. In comparison with the literature, Dudonne and collaborators evaluated the antioxidant activity of 30 aqueous plant extracts, including the extract from *Eucalyptus globulus* leaves. In the study on FRAP, for Eucalyptus extract, a value of 4.66 mmol g<sup>-1</sup> was obtained, which classified it among the best potential antioxidants (Dudonné *et al.*, 2009). Thus, the FRAP value obtained in this study is higher than the value described in the literature, with variations occurring due to different forms of extraction, different analyzed species, as well as times of the year, location and season of harvesting the leaves.

To evaluate the composition of the Fe(NPs), X-ray diffractometry (XRD) was employed. Firstly, Figure 2 shows Fe(NPs) 0% (without vegetable coating).

In this sample, it was possible to observe characteristic peaks of lepidocrocite (FeO(OH)) (JCPDS44-1415), with an orthorhombic arrangement, magnetite (Fe<sub>3</sub>O<sub>4</sub>) (JCPDS75-1609), with a cubic arrangement, and iron hydroxide oxide (FeO(OH)) (JCPDS26-0792), with orthorhombic crystals (Dong *et al.*, 2016; 2017; Bibi *et al.*, 2019).

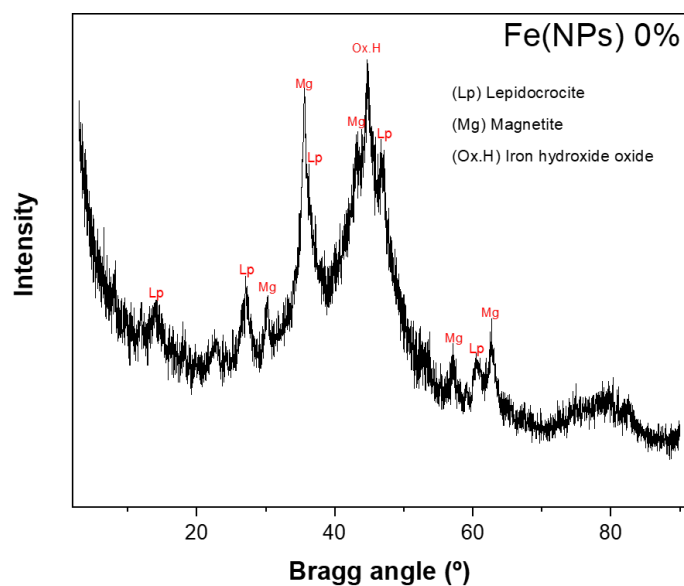


**Figure 2.** X-ray diffraction of Fe(NPs) 0%.

Figure 3 shows the XRD of the nanoparticles coated with Eucalyptus extract:

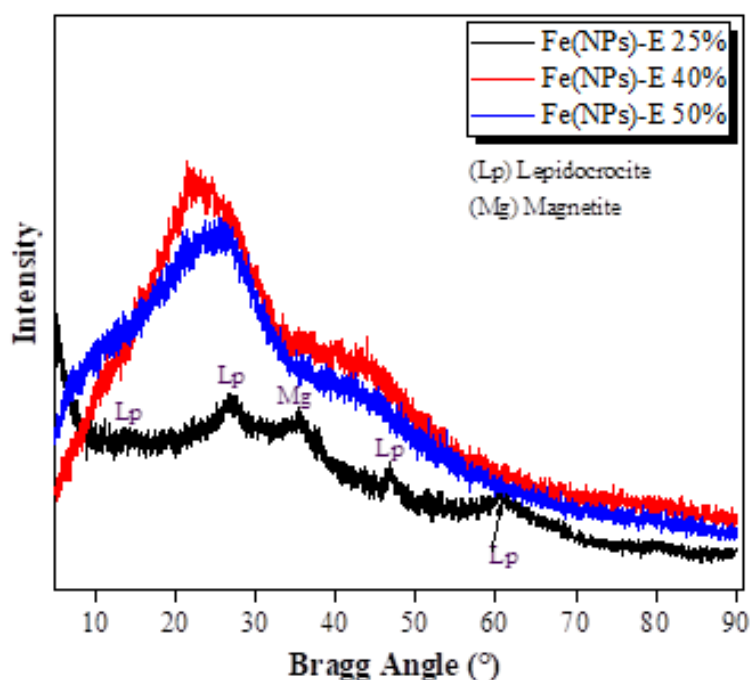


**Figure 3.** X-ray diffraction patterns of the samples Fe(NPs)-E 25%, Fe(NPs)-E 40% and Fe(NPs)-E 50%.

Fe(NPs)-E 25% exhibits peaks characteristic of lepidocrocite ( $\text{FeO}(\text{OH})$ )(JCPDS44-1415), and a peak referring to the magnetite phase ( $\text{Fe}_3\text{O}_4$ )(JCPDS19-0629). Fe(NPs)-E 40% and Fe(NPs)-E 50% were amorphous, which can be attributed to the higher volumetric proportion of the plant extract, resulting in decreased crystallinity. When we compare the Fe(NPs)-E 25% and Fe(NPs) 0% X-ray diffraction patterns, it is possible to notice that both have peaks characteristic of lepidocrocite, but the difference is that there is a decrease in the number of magnetite signals for the Fe(NPs)-E 25%. Therefore, it is possible to state that the use of a greater volumetric proportion of the plant extract promotes significant changes in the composition and crystallinity of Fe(NPs) (Dong *et al.* 2016; 2017; Bibi *et al.*, 2019).

### 3.2. Vegetable coatings (FTIR)

Figure 4 depicts the FTIR spectra of the samples Fe(NPs)-E 25%, Fe(NPs)-E 40%, and Fe(NPs)-E 50%, which feature vegetable coatings from Eucalyptus leaves. First, in all the spectra, bands near  $500\text{ cm}^{-1}$  related to the Fe-O bond of the metallic cores are observed (Singh *et al.*, 2016). Additionally, bands in the region between  $900$  and  $1200\text{ cm}^{-1}$ , associated with the plant coating, specifically the C-O bond of alcohols and ethers (Maikudi *et al.*, 2021), are present. The bands at  $1440\text{ cm}^{-1}$  and  $1600\text{ cm}^{-1}$  also indicate the C=C bond in aromatic compounds (Maikudi *et al.*, 2021), while the band at  $3350\text{ cm}^{-1}$  is possibly attributed to the stretching vibration of the O-H group or the O-H bond of alcohols and carboxylic acids (Maikudi *et al.*, 2021), is also observed in all three samples.

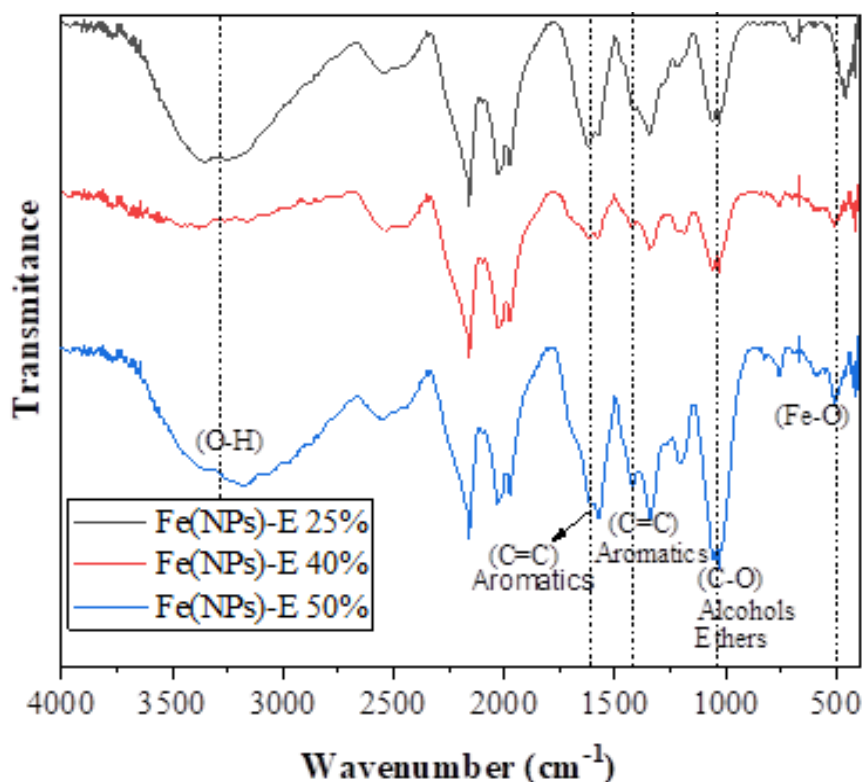


**Figure 4.** FTIR spectra of iron nanoparticles coated with Eucalyptus extract.

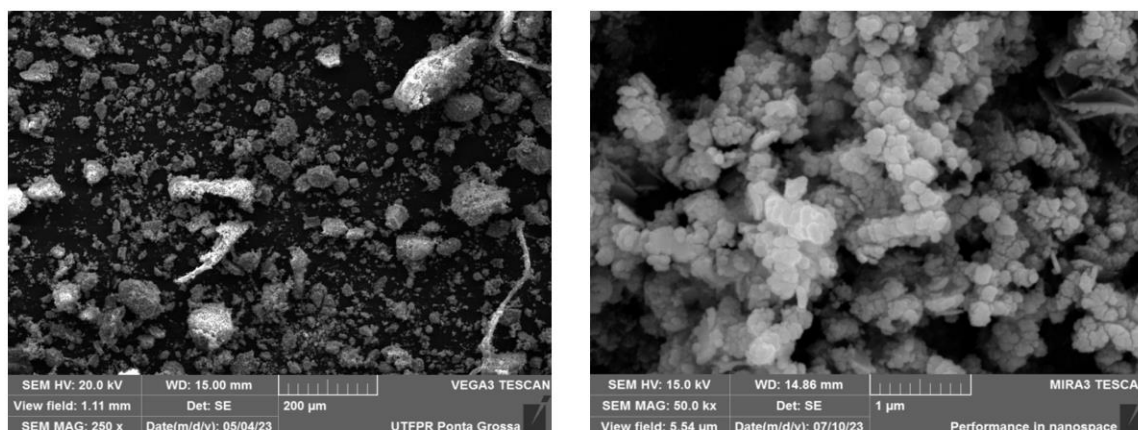
Evaluating the presence of bands related to the Eucalyptus leaf extract, it can be stated that the coating was effective, acting to stabilize the particles. Furthermore, the analysis indicates the presence of bonds related to phenolic compounds, carboxylic and aromatic acids.

### 3.3. Particle evaluation (SEM/EDS and HR-FESEM)

SEM and HR-FESEM analyses were employed to conduct a qualitative evaluation of the structures of Fe(NPs). The utilization of both analyses was motivated by their distinct magnification potentials. SEM analysis enabled a comparative assessment of particle sizes and irregular morphologies, whereas HR-FESEM facilitated the evaluation of fissure and pore presence.

Figure 5 shows the SEM and HR-FESEM of the Fe(NPs) 0% at magnifications of 250 x and 50 kx. In the figure at 250x magnification, it is possible to assess that the material has an irregular size related to the lack of a coating agent, so the particles tend to clump together. At the magnification of 50 kx, the presence of cracks and pores is observed, which may be ideal for Fe(NPs) 0% to act in adsorption processes.



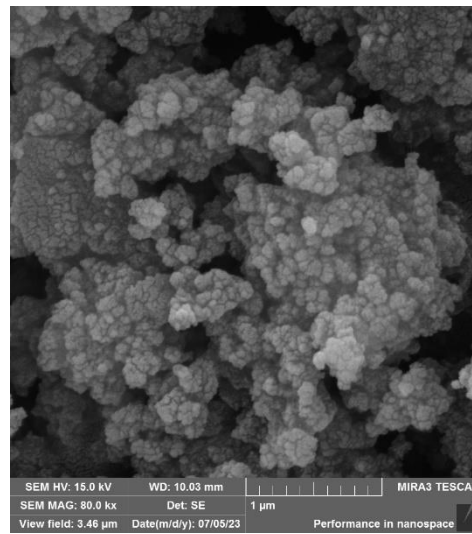
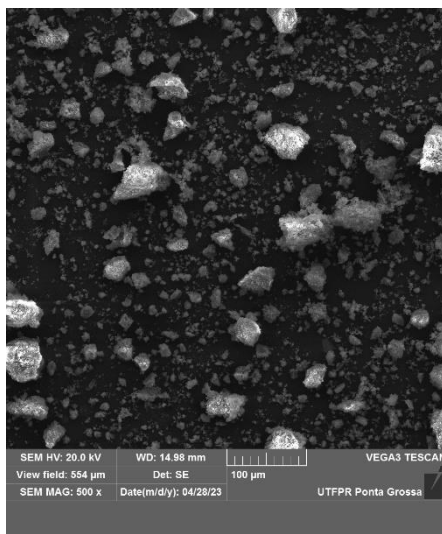
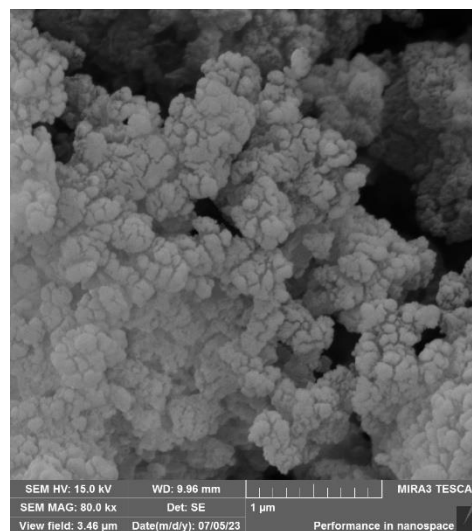
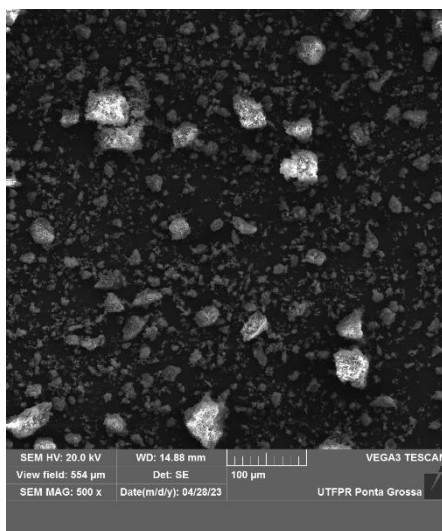
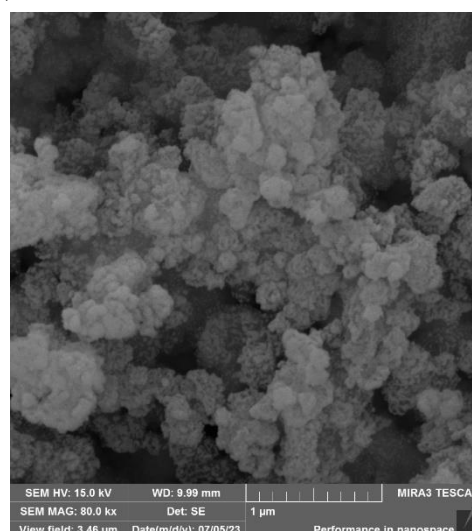
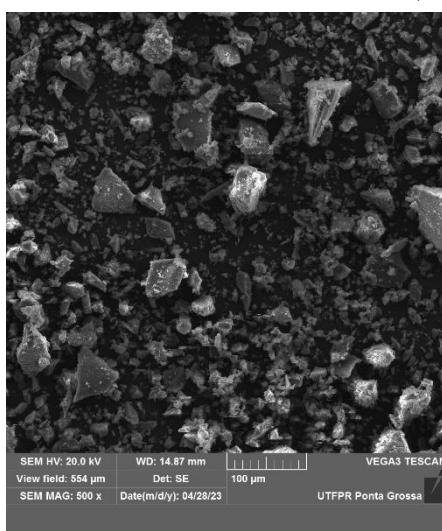


**Figure 5.** SEM and HR-FESEM of Fe(NPs) 0%.

Figure 6 shows the SEM and HR-FESEM images, with magnifications of 500 x and 80 kx, of the samples coated with Eucalyptus extract. At 500 x magnifications, irregular particle sizes and shapes were observed across the three samples, likely due to the presence of the plant extract in the synthesis process. The extract, being a complex matrix rich in various compounds, complicates the control over particle size and morphology, leading to variability. However, upon comparative analysis, similar particle sizes were noted for all four Fe(NPs) samples, suggesting that the presence of different volumetric proportions of the extract did not significantly alter the particle size. Additionally, at 80 kx magnification of the coated samples, the presence of cracks or pores was again observed, indicating the material's potential as an effective adsorbent.

Similarly, Mokshith *et al.* (2022) conducted green synthesis of Fe(NPs) using the extract of *Hymenocallis littoralis* flowers. In the study, Fe(NPs) with irregular shapes and sizes ranging from 120 to 200 nm were obtained (Mokshith *et al.*, 2022). In another study, Nahari *et al.* (2022) promoted the synthesis of Fe(NPs) also through the green method, employing the aqueous extract of *Vitex leucoxylo*n leaves. In this case, the synthesized nanoparticles also exhibited variations in size (45 to 100 nm), however, the Fe(NPs) displayed spherical shapes (Nahari *et al.*, 2022). In both cases, the presence of diverse shapes and primarily varied sizes could be attributed to the rich matrix of the employed plant extracts in the synthesis process.

In addition to SEM, EDS analysis allows for the evaluation of iron ions present in the samples (Figure 7). In this context, the presence of these ions is evident in the EDS of all samples, which are crucial to ensuring good catalytic activities due to their versatility in catalyzing various reactions and their capacity to form complexes with several organic molecules, thereby providing a favorable reactive environment (Kharisov *et al.*, 2016). In this context, thermal analysis will enable the quantitative assessment of iron ions, elucidating whether variations in the volumetric proportions of the syntheses have led to alterations in the presence of these ions from one nanoparticle to another.

**Fe(NPs)-E 25%****Fe(NPs)-E 40%****Fe(NPs)-E 50%**

**Figure 6.** SEM and HR-FESEM images of Fe(NPs) coated with Eucalyptus extract, magnifications of 500 x and 80 kx.

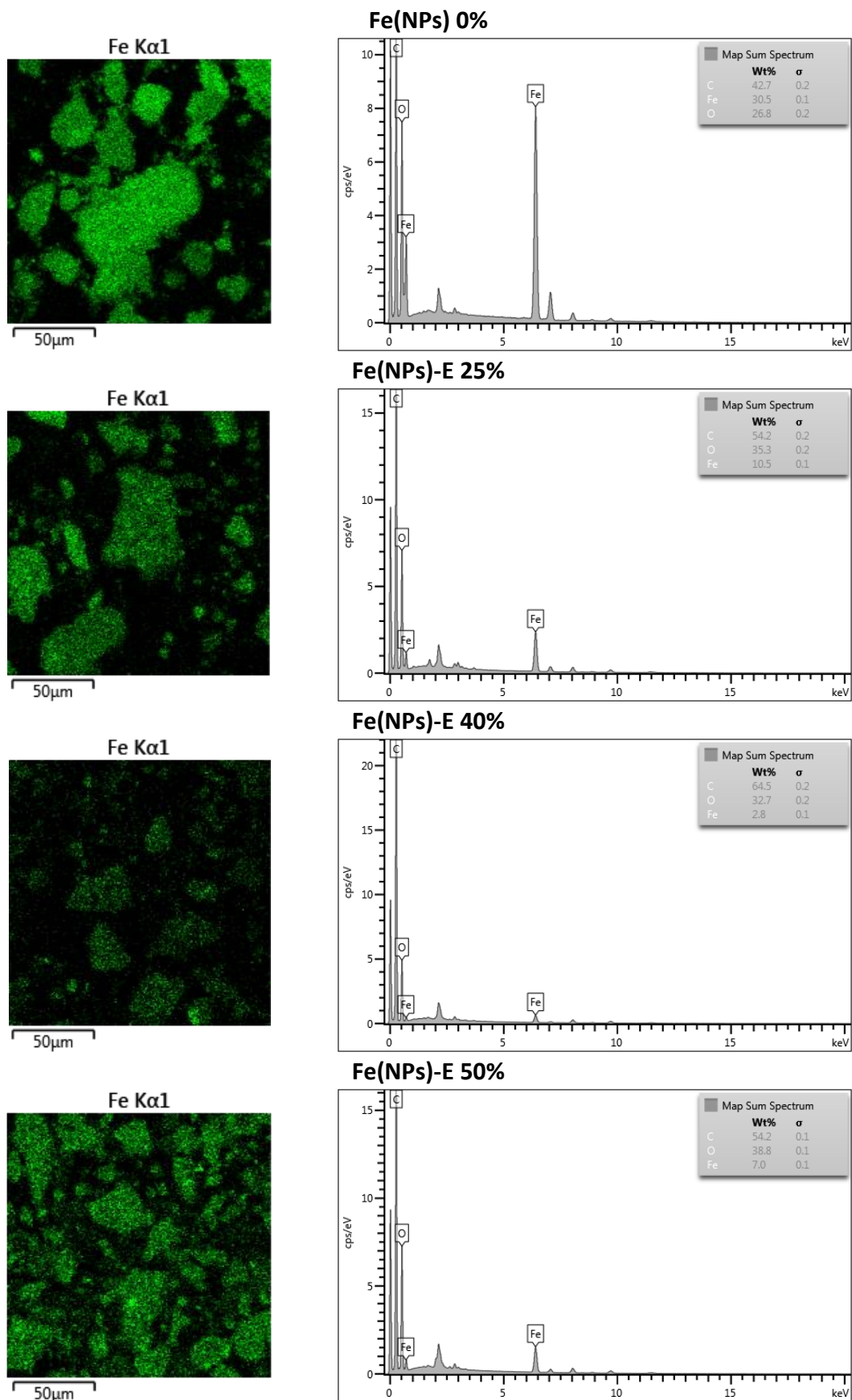
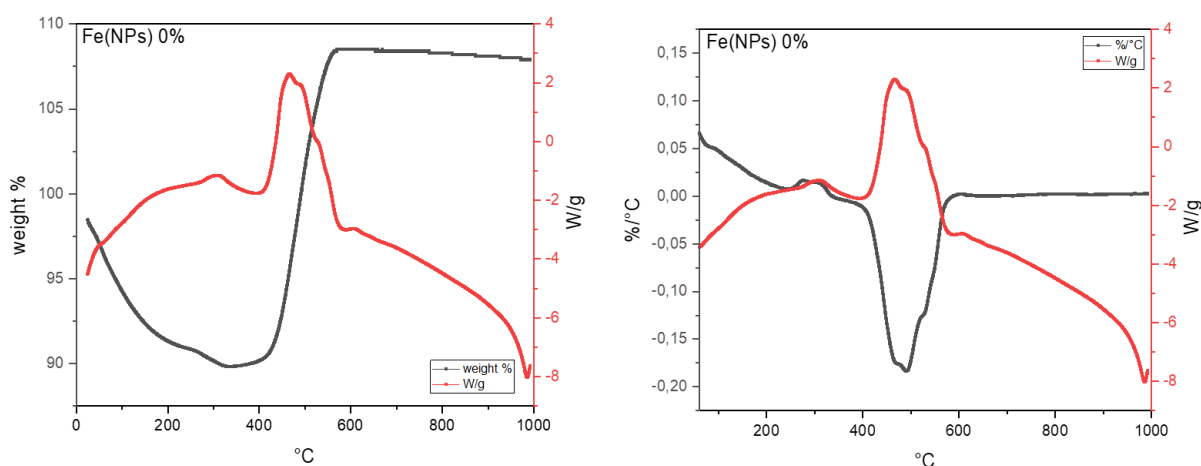


Figure 7. EDS of Fe(NPs).



### 3.4. Thermal analysis

Figure 8 shows the thermal analysis (TGA and DTA) of the Fe(NPs) 0%. With the aid of thermogravimetric analysis (TGA), a gradual loss of 11.3% of the mass is observed from the initial temperature up to 350°C, which is possibly related to the adsorbed water molecules and the hydrogens associated with the lepidocrocite and iron hydroxide oxide phases. Furthermore, after the loss, there is a gain in mass, reaching 108.4%, referring to the oxidation of the material to the hematite phase ( $\alpha$ -Fe<sub>2</sub>O<sub>3</sub>). Additionally, TGA was used to calculate the mass of iron in the sample, resulting in 7.34 mg of iron. Finally, in Differential Thermal Analysis (DTA), an exothermic signal is noted at 470°C related, again, to mass loss.



**Figure 8.** Thermal analysis of the Fe(NPs) 0% sample.

Figure 9 shows the thermal analysis of the samples coated with Eucalyptus extract. It is observed that all samples present mass losses from the initial temperature up to approximately 400°C related to the adsorbed water molecules and the loss of the organic portion associated with the Eucalyptus plant extract. Unlike the other samples, Fe(NPs)-E 25% does not show such a pronounced mass loss. A loss of approximately 43.9%, which is related to the oxidation of the material to hematite ( $\alpha$ -Fe<sub>2</sub>O<sub>3</sub>). For the samples Fe(NPs)-E 40% and Fe(NPs)-E 50%, the mass loss is accentuated, approximately 73.6% and 84.1%, possibly because the material is oxidized, and in this way, there is no mass gain due to the addition of the oxygen species. Now, regarding the mass of iron, 3.68, 1.56 and 0.9 mg were calculated for Fe(NPs)-E 25%, Fe(NPs)-E 40% and Fe(NPs)-E 50%, respectively. The loss of mass occurs up to a high temperature, an indication that the organic portion and the other compounds were strongly linked to the metallic nuclei.

Concerning DTA, Fe(NPs)-E 25% presents an exothermic signal at 300°C, while Fe(NPs)-E 40% has two exothermic signals at 210 and 260°C, and finally, Fe(NPs)-E 50% has an exothermic signal at 380°C. Therefore, all exothermic signals are associated with the mass losses of Fe(NPs) coated with Eucalyptus extract.

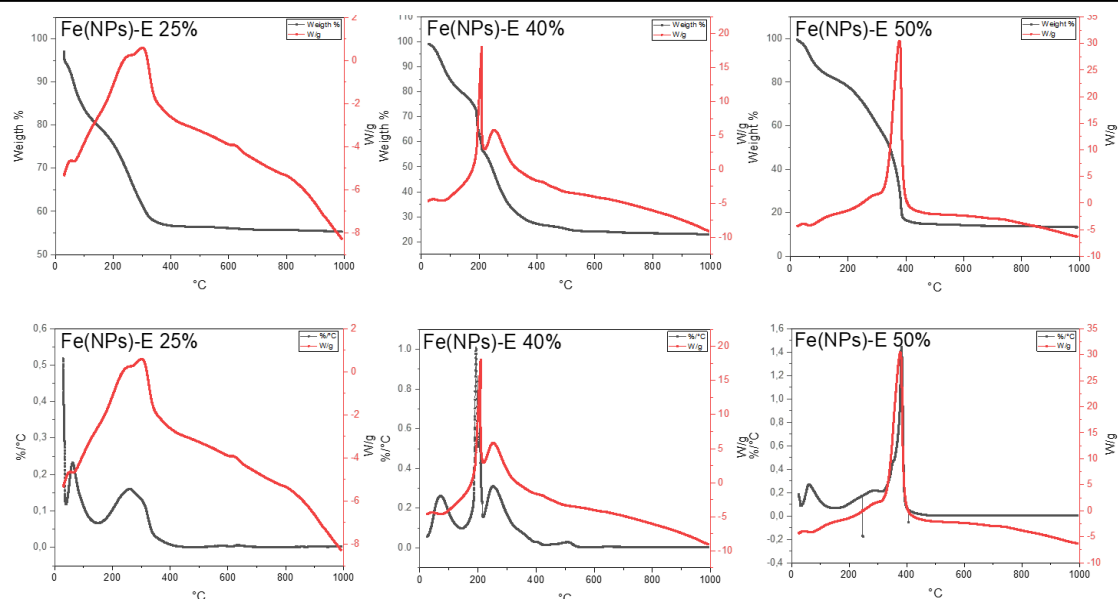


**Figure 9.** Thermal analysis of the iron nanoparticles coated with Eucalyptus extract.

### 3.5. BET

Figure 10 displays the sorption isotherms of Fe(NPs). The samples Fe(NPs) 0% and Fe(NPs)-E 25% exhibit type IV isotherms characterized by H3 hysteresis loops. This phenomenon is indicative of mesoporous behavior, where adsorption is attributed to specific adsorptive interactions between the adsorbate and the internal surface of the pores. It is observed that initial adsorption is gradual at low relative pressures, followed by rapid adsorption at higher pressures. The presence of H3-type hysteresis is associated with a phenomenon suggesting an indefinite distribution in pore size and shape (Amos-Tautua *et al.*, 2020; Fekry *et al.*, 2023).

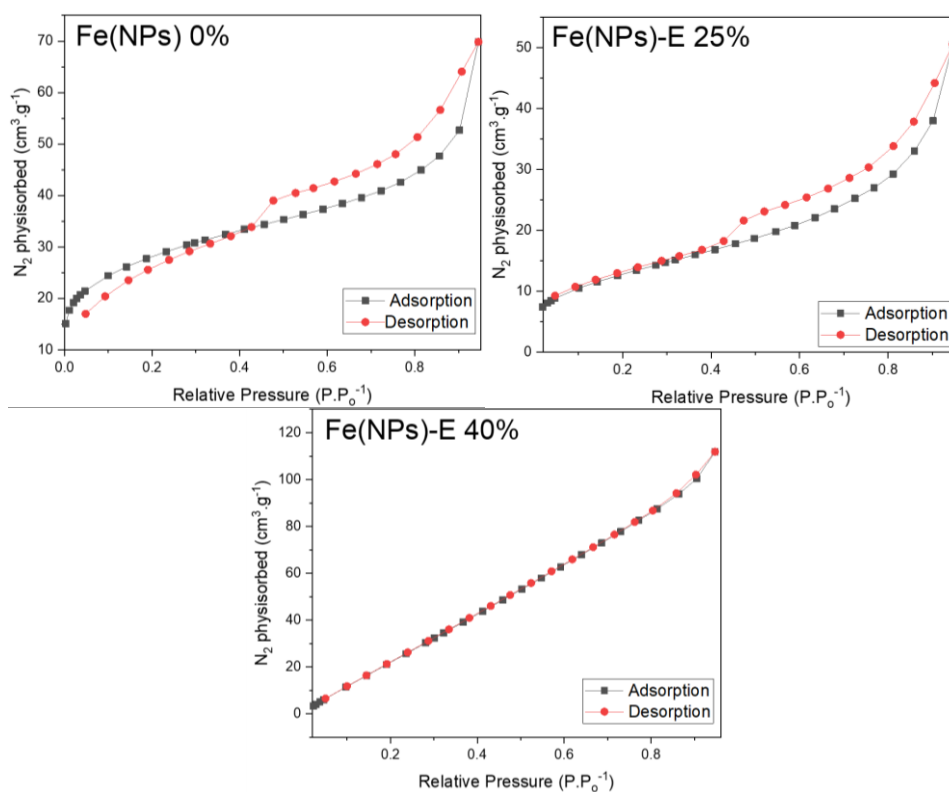


**Figure 10.** Sorption isotherms of Fe(NPs).



Fe(NPs)-E 40% exhibits a Type III isotherm, characterized by the rapid and continuous accumulation of adsorbed gas on the solid surface across the entire range of investigated pressures, without the discernible presence of an adsorption plateau. This pattern is attributed to relatively weak interactions between the adsorbent and the adsorbate (Atran *et al.*, 2024).

Figure 11 displays the pore size distributions of the Fe(NPs). Fe(NPs) 0%, Fe(NPs)-E 25% and Fe(NPs)-E 40% exhibit similar behavior patterns, characterized by high concentrations of pores around approximately 1.8 nm, suggesting heterogeneous distributions. These pore distribution patterns are reflected in the different isotherms obtained between the samples. Fe(NPs) 0% and Fe(NPs)-E 25% exhibit similar isotherms, correlated with similar pore distributions, which include significant amounts of micropores and the presence of mesopores. Additionally, although Fe(NPs)-E 40% displays behavior partly similar to Fe(NPs) 0% and Fe(NPs)-E 25%, with a heterogeneous distribution of pores and predominance of micropores and mesopores, the obtained isotherm is of Type III, primarily reflecting changes in pore morphology.

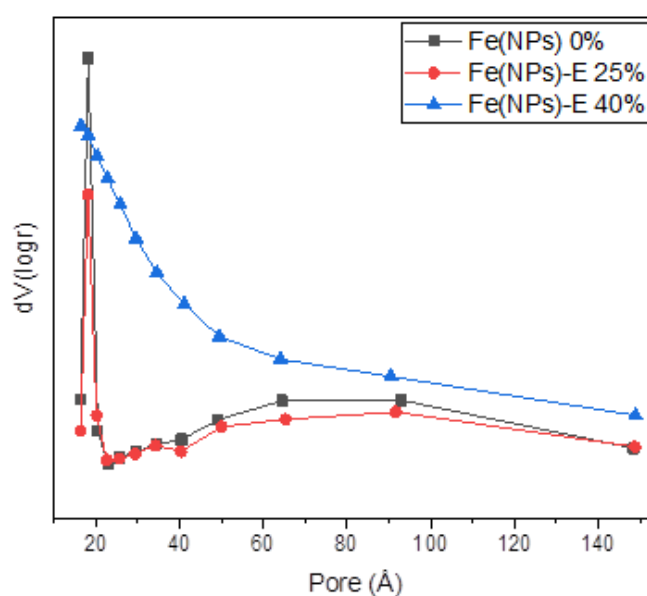


**Figure 11.** Pore-size distributions of the Fe(NPs).

Table 2 presents the textural properties of the Fe(NPs) determined by N<sub>2</sub> physisorption. Initially, it is observed that Fe(NPs)-E 40% exhibits the highest surface area, followed by Fe(NPs) 0%, and subsequently by Fe(NPs)-E 25%. Surface area is a crucial parameter used to understand properties such as adsorption capacity, chemical reactivity, and dissolution rate, among others. It is widely recognized that nanoparticles with excellent surface areas often exhibit significant catalytic activities due to the increased surface contact between the nanoparticles and their surrounding environment. The ability of these nanoparticles to efficiently interact with the environment, owing to their vast surface area, is one of the main reasons they are studied in various scientific disciplines and find diverse applications.

**Table 2.** Textural properties of the Fe(NPs) determined by N<sub>2</sub> physisorption at 250°C.

Samples	Specific area (m <sup>2</sup> g <sup>-1</sup> )	Pore volume (cm <sup>3</sup> g <sup>-1</sup> )	Average pore size (nm)
Fe(NPs) 0%	95.6	0.08	1.8
Fe(NPs)-E 25%	46.7	0.07	1.8
Fe(NPs)-E 40%	160.3	0.2	1.6

Regarding the pore volumes, it is observed that Fe(NPs) 0% and Fe(NPs)-E 25% exhibit very similar pore volume values. On the other hand, Fe(NPs)-E 40% showed pores with significantly larger volumes compared to the other Fe(NPs). This disparity is related to the higher surface area obtained by Fe(NPs)-E 40%, which may provide enhanced properties for storage or transportation of substances.

Finally, the Fe(NPs) exhibited quite similar average pore sizes, ranging from 1.6 to 1.8 nm, which characterizes the predominance of micropores.

### 3.6. Catalytic activity

Catalytic reduction of 4-nitrophenol was used to evaluate the catalytic activity of the Fe(NPs), observing how the different volumetric proportions of the plant extract and NaBH<sub>4</sub> can affect this factor. Initially, in the process, the hydrogens released by the NaBH<sub>4</sub> molecules are incorporated into Fe(NPs), which act as catalysts. As a result, the 4-nitrophenolate molecules also bind to the catalysts (Fe(NPs)) that are rich in hydrogens. Afterward, the hydrogens from the catalysts are transferred to the 4-nitrophenolate ions, and then occurs the reduction to 4-aminophenol, which characterizes a chemical adsorption with a change in the structure of the adsorbate (Wunder *et al.*, 2010). Furthermore, NaBH<sub>4</sub> acts as a reducing agent in the process and in the alkalization of the reaction medium, converting 4-nitrophenol into 4-nitrophenolate, a compound more susceptible to reduction. Sravanthi *et al.* (2019) assessed that in the absence of NaBH<sub>4</sub> there is no conversion of 4-nitrophenol to 4-aminophenol after a period of 24 hours. It is still necessary to emphasize that the presence of catalysts is essential to accelerate the reduction process (Sravanthi *et al.*, 2019).

In the procedures, initial concentrations of 10 mg L<sup>-1</sup> of 4-nitrophenolate and 40 mg of Fe(NPs) were used. Figure 12 shows the concentration of the 4-nitrophenolate as a function of reaction time.

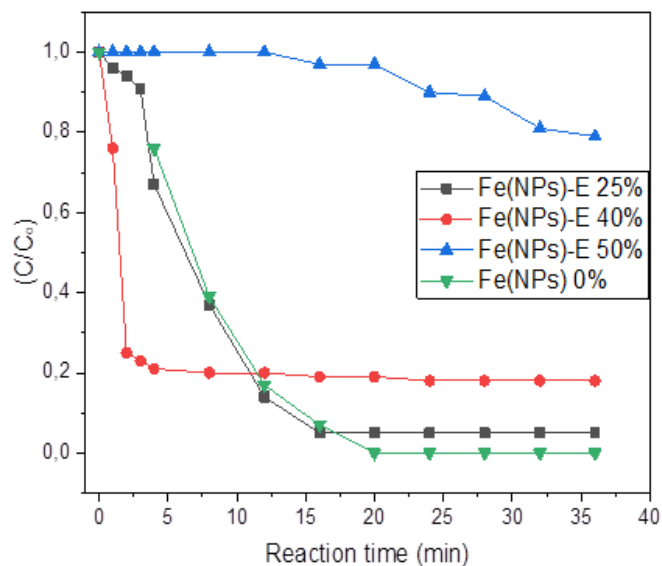


**Figure 12.** Concentration of 4-nitrophenolate ions as a function of catalytic reduction reaction time.

Table 3 presents the obtained conversions as a function of reaction time. It is possible to observe that Fe(NPs) 0% was the one that achieved the best performance, being able to catalyze a conversion of 100% in 20 minutes, which was expected, considering that Fe(NPs) formed by the chemical methods typically have high catalytic performances. Another point is that the vegetable coating forms a blockage on the nanoparticle surface that is ideal against agglomerations and oxidation, but can affect the material's performance in catalytic processes. However, Fe(NPs)-E 25% and Fe(NPs)-E 40% also showed good results, resulting in

conversions of 95% and 82% after 16 and 24 minutes, respectively. Therefore, the vegetable coatings of these nanoparticles, Fe(NPs)-E 25% and Fe(NPs)-E 40%, did not significantly affect the catalytic performances and were ideal for stabilization. For the Fe(NPs)-E 50%, the conversion was 21% after 36 minutes, and therefore, was lower than expected, possibly because the synthesis of Fe(NPs)-E 50% does not have the presence of the chemical agent.

**Table 3.** Conversions achieved with the iron nanoparticles.

Nanoparticles	Conversion (%)	Reaction time (min)
Fe(NPs) 0%	100	20
Fe(NPs)-E 25%	95	16
Fe(NPs)-E 40%	82	24
Fe(NPs)-E 50%	21	36

Figure 13 presents the scans obtained in UV-VIS related to each catalytic reduction.

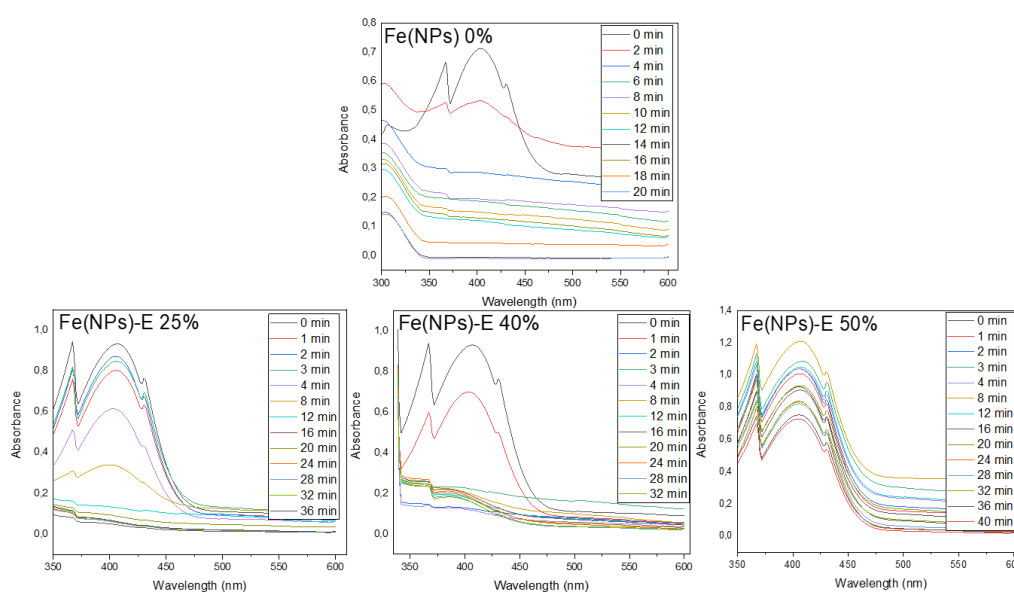


**Figure 13.** Scans (UV-VIS) related to catalytic reductions.

In general, a decrease in the signal at 400 nm is observed in the scans, which characterizes the conversion of 4-nitrophenolate. Therefore, the decrease in signal intensity occurs according to the previously mentioned catalytic potential, which varies from one nanoparticle to another.

On the other hand, the first-order model was employed to model the reduction kinetics of 4-nitrophenol, following the equation  $\ln(C_0/C) = K_r t$ , where "C" is the concentration at any time "x", "C<sub>0</sub>" is the initial concentration, "K<sub>r</sub>" is the reduction constant, and "t" is time. Table 4 displays the reduction constants and coefficients of determination (R<sup>2</sup>) obtained for each nanoparticle (Bhole *et al.*, 2023).

**Table 4.** Reduction constants and coefficients of determination (R<sup>2</sup>) obtained for each nanoparticle.

Nanoparticle	K <sub>r</sub> (min <sup>-1</sup> )	R <sup>2</sup>
Fe(NPs) 0%	0.22	0.98
Fe(NPs)-E 25%	0.19	0.97
Fe(NPs)-E 40%	0.11	0.50
Fe(NPs)-E 50%	0.01	0.94

It is observed that Fe(NPs)-E 40% did not show a good fit by the first-order model, exhibiting an  $R^2$  of 0.5. Therefore, this model was not the most suitable to represent the kinetic behavior of Fe(NPs)-E 40%. However, the other Fe(NPs) showed good fits by the first-order kinetics, with  $R^2$  values greater than 0.94. Fe(NPs) 0% and Fe(NPs)-E 25% exhibited the highest reduction rates over time, i.e., higher "Kr" values, while Fe(NPs)-E 50% exhibited the poorest reduction rate.

### 3.7. Ecotoxicological test

#### 3.7.1. Brine shrimp

Figure 14 shows the ecotoxicological test regarding the trophic level of microcrustaceans. In the graph, the "y" axis relates to the unit of dead microcrustaceans and the "x" axis to the average of each sample. Regarding the "Tukey" test, the results have significant variations between them, with  $p < 0.05$ . To evaluate the toxicity of each sample, the effective concentration ( $EC_{20}$ ) was considered, which, according to the current legislation, for an average mortality greater than 20%, that is, 2 brine shrimp, was considered a toxic effect. Therefore, both  $NaBH_4$  and 4-nitrophenol (4NF) hurt this trophic level, with an average mortality of approximately 9 and 4 individuals, respectively. However, after catalytic reduction, the contaminant showed a reduction in its toxicity, presenting an average mortality of 1 individual for Fe(NPs)-E 40%; therefore, the value is within that allowed by current legislation. Regarding leachate, both the coated leachate (Fe(NPs)-E 25%) and the uncoated leachate (Fe(NPs) 0%) present average mortality values within the allowable range, with approximately 1 and 0.5 of microcrustaceans dead.

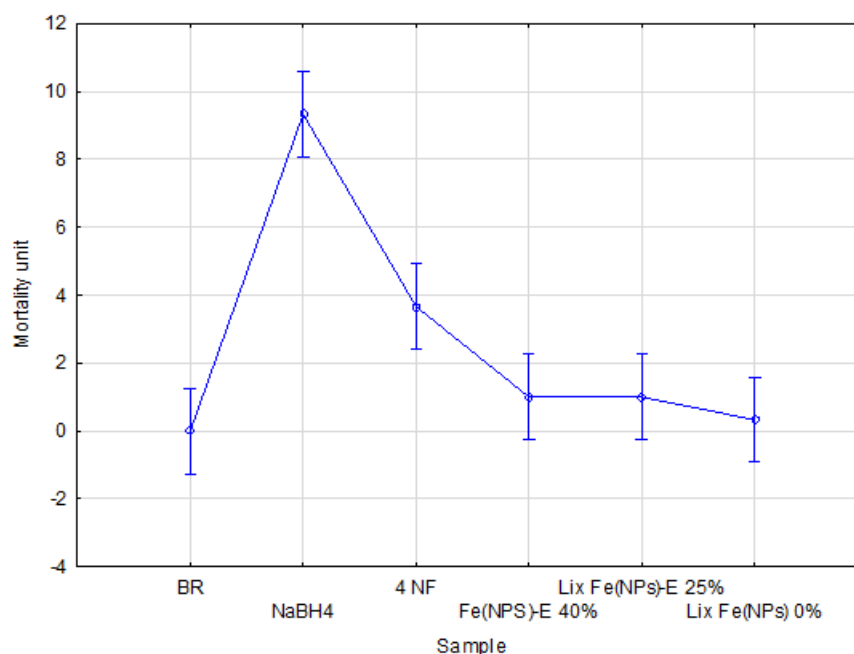


**Figure 14.** Ecotoxicological test on the trophic level of microcrustaceans.

Furthermore, the ecotoxicological test was ideal to represent the high toxicity of the chemical agent ( $NaBH_4$ ), and therefore the importance of seeking alternative methods to replace or minimize the use of this contaminant.

#### 3.7.2. Lemna minor

Concerning the ecotoxicological test on the trophic level of aquatic plants (Figure 15), the "y" axis shows the variation in the number of fronds and the "x" axis is the average for each sample. A significant variation is observed between the obtained values; therefore the "Tukey"

test presents  $p < 0.05$ . To evaluate the toxicity of each sample, the effective concentration ( $EC_{20}$ ) was considered again, in which in this case, a negative variation greater than -2 fronds was judged as toxic. Therefore, the white obtained a positive variation of 0.25 fronds, which indicates that even without the tested samples, Lemna did not have a high cloning rate, which may have occurred due to the low temperature during the days of analysis. Regarding the samples, 4-nitrophenol (4NF), before reduction, obtained a negative variation of -3.75 fronds, and was then considered toxic for this trophic level.

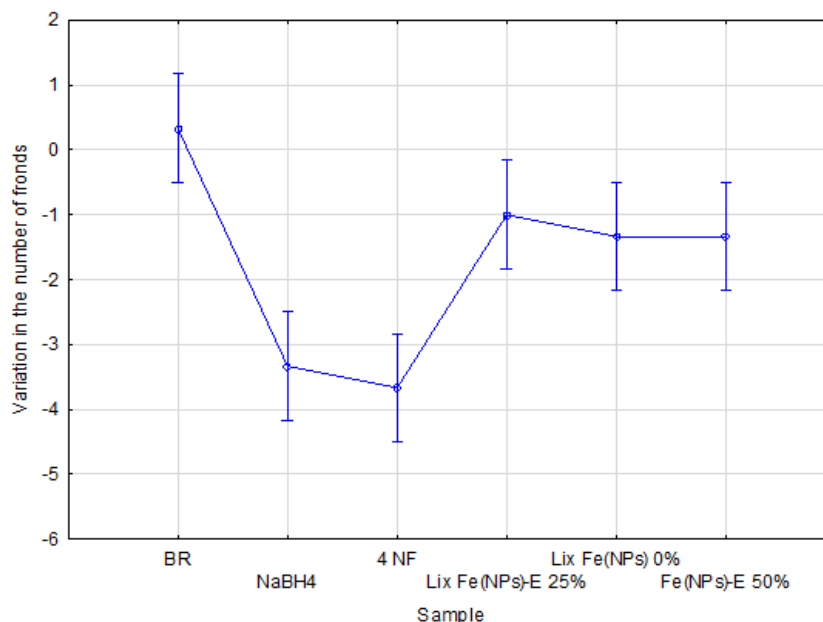


**Figure 15.** Ecotoxicological test with trophic level of aquatic plants.

After catalytic reduction, Fe(NPs)-E 50% was not considered toxic with a variation of -1.25 fronds, and therefore the catalytic treatment was judged effective in reducing the toxicity of 4-nitrophenol, obtaining a value permitted by current legislation. Furthermore, the leachates, Fe(NPs)-E 25% and Fe(NPs) 0%, were not toxic to aquatic plants with a variation of -1 and -1.25 fronds, respectively, which indicates the good compatibility of nanoparticles formed with the trophic level. Finally, the toxicity of the chemical agent,  $NaBH_4$ , was evaluated and a variation of -3.25 fronds was obtained, an indication of the need to seek alternative synthesis methods that minimize or replace the use of this compound.

## 4. CONCLUSIONS

The application of an alternative methodology, green synthesis, through a simple, cheap and sustainable process was ideal for synthesizing Fe(NPs). The use of a volumetric proportion of up to 25% of the plant extract generated Fe(NPs) with a certain crystallinity, however, for higher proportions the formed materials were amorphous. Further, the particle sizes were not significantly changed by the different volumetric proportions used. The vegetable coating was effective, observed by FTIR through characteristic bands of aromatic compounds, alcohols, ethers and carboxylic acids. Observing the thermal analyses, it was possible to quantify the mass of iron present in each sample; thus, in relation to the mass  $Fe(NPs) 0\% > Fe(NPs)-E 25\% > Fe(NPs)-E 40\% > Fe(NPs)-E 50\%$ . Finally, the Fe(NPs) formed showed good catalytic performances for volumetric proportions of up to 40% of the plant extract from Eucalyptus leaves, acting in the catalysis of reduction of 4-nitrophenol, which was ideal for reducing the toxicity of the compound according to ecotoxicological tests.



The excellent catalytic activities exhibited by the Fe(NPs) with up to 40% of the vegetal extract are possibly associated, among other factors, with the optimal surface areas obtained, as observed through BET analysis. Furthermore, the good biocompatibility of Fe(NPs) was exposed in ecotoxicological tests, as was the high toxicity of the chemical agent NaBH<sub>4</sub>, which highlights the need to seek alternative synthesis methods that replace or minimize the use of the compound.

## 5. ACKNOWLEDGMENTS

I would like to thank my supervisors, Marcio Barreto Rodrigues and Rodrigo Brackmann for their support, for always encouraging my professional development and my research in general. Furthermore, I record my gratitude to Andressa Pilonetto, Raquel Dalla Costa da Rocha and Yasmin Milena Loth Bueno, for helping with the experiments developed. It is also necessary to highlight my affection and gratitude to the Soil Laboratory and the Multiuser Central Analysis Laboratory, Pato Branco campus, which provided the space, reagents and equipment necessary for research.

Last but not least, I thank the Federal Technological University of Paraná (Pato Branco and Ponta Grossa campuses), Postgraduate Program in Chemical and Biochemical Process Technology (PPGTP), and the Coordination for Personal Improvement of Higher Education – Brazil (CAPES) – Financing Code 001 for the financial support.

## 6. REFERENCES

- AMOS-TAUTUA, B. M. *et al* Effect of synthetic conditions on the crystallinity, porosity and magnetic properties of gluconic acid capped iron oxide nanoparticles. **Nano-Structures and Nano-Objects**, v. 23, p. 100480, 2020. <https://doi.org/10.1016/j.nanoso.2020.100480>
- ATRAN, A. A. *et al* Iron incorporated porous cerium oxide nanoparticles as an efficient photocatalyst for different hazardous elimination. **Journal of Rare Earths**, 2024. <https://doi.org/10.1016/j.jre.2024.02.006>
- BIBI, I. *et al* Green synthesis of iron oxide nanoparticles using pomegranate seeds extract and photocatalytic activity evaluation for the degradation of textile dye. **Journal of Materials Research and Technology**, v. 8, n. 6, p. 6115–6124, 2019. <https://doi.org/10.1016/j.jmrt.2019.10.006>
- BHOLE, R. *et al* Superparamagnetic spherical magnetite nanoparticles: synthesis, characterization and catalytic potential. **Applied Nanoscience Switzerland**, v. 13, n. 9, p. 6003–6014, 2023. <https://doi.org/10.1007/s13204-022-02532-4>
- CHUNG, I. M. *et al* Plant-Mediated Synthesis of Silver Nanoparticles: Their Characteristic Properties and Therapeutic Applications. **Nanoscale Research Letters**, v. 11, n. 1, p. 1–14, 2016. <http://dx.doi.org/10.1186/s11671-016-1257-4>
- DONG, H. *et al* Aging study on carboxymethyl cellulose-coated zero-valent iron nanoparticles in water: Chemical transformation and structural evolution. **Journal of Hazardous Materials**, v. 312, p. 234–242, 2016. <https://doi.org/10.1016/j.jhazmat.2016.03.069>
- DONG, H. *et al* Physicochemical transformation of carboxymethyl cellulose-coated zero-valent iron nanoparticles (nZVI) in simulated groundwater under anaerobic conditions. **Separation and Purification Technology**, v. 175, p. 376–383, 2017. <https://doi.org/10.1016/j.seppur.2016.11.053>

- DUDONNÉ, S. *et al* Comparative study of antioxidant properties and total phenolic content of 30 plant extracts of industrial interest using DPPH, ABTS, FRAP, SOD, and ORAC assays. **Journal of Agricultural and Food Chemistry**, v. 57, n. 5, pag. 1768–1774, 2009. <https://doi.org/10.1021/jf803011r>
- FEKRY, M. *et al* Impact of poly naphthalene sulfonate on the dispersion stability of iron oxide nanoparticles. **Egyptian Journal of Petroleum**, v. 32, n. 1, p. 23–32, 2023. <https://doi.org/10.1016/j.ejpe.2023.01.001>
- KE, H. *et al* Factors controlling pure-phase multiferroic BiFeO<sub>3</sub> powders synthesized by chemical co-precipitation. **Journal of Alloys and Compounds**, v. 509, n. 5, p. 2192–2197, 2011. <http://dx.doi.org/10.1016/j.jallcom.2010.09.213>
- KHAIRUL, H. M. N. M.; SAPAWE, N. A short review on green synthesis of iron metal nanoparticles via plant extracts. **Materials Today: Proceedings**, v. 31, p. A48–A53, 2020. <https://doi.org/10.1016/j.matpr.2020.10.968>
- KHARISOV, B. I. *et al* Iron-based Nanomaterials in the Catalysis. **Advanced Catalytic Materials - Photocatalysis and Other Current Trends**, n. January 2017, p. 36-68, 2016. <http://dx.doi.org/10.5772/61862>
- MAIKUDI, M. *et al*. Journal of Pharmacy and Chemistry. **Journal of Tropical Pharmacy and Chemistry**, v. 5, n. 4, p. 396–405, 2021. <https://jtpc.farmasi.unmul.ac.id>
- MOHANTY, U. S. Electrodeposition: A versatile and inexpensive tool for the synthesis of nanoparticles, nanorods, nanowires, and nanoclusters of metals. **Journal of Applied Electrochemistry**, v. 41, n. 3, p. 257–270, 2011. <https://doi.org/10.1007/s10800-010-0234-3>
- MOKSHITH, D. G.; KALPASHREE, M. M.; KRISHNA, D. K. Natural Synthesis of Nanoparticles using Flower Extract of *Hymenocallis littoralis* (Jacq) Salisb and Evaluation of its Antimicrobial activity. **International Journal for Research in Applied Science and Engineering Technology**, v. 10, n. 10, p. 1199–1207, 2022. <https://doi.org/10.22214/ijras.2022.47158>
- NAHARI, M. H. *et al* Green Synthesis and Characterization of Iron Nanoparticles Synthesized from Aqueous Leaf Extract of *Vitex leucoxydon* and Its Biomedical Applications. **Nanomaterials**, v. 12, n. 14, 2022. <https://10.3390/nano12142404>
- NAIKOO, G. A. *et al* Bioinspired and green synthesis of nanoparticles from plant extracts with antiviral and antimicrobial properties: A critical review. **Journal of Saudi Chemical Society**, v. 25, n. 9, p. 101304, 2021. <https://doi.org/10.1016/j.jscs.2021.101304>
- SALVADOR, M. *et al* Microemulsion synthesis of superparamagnetic nanoparticles for bioapplications. **International Journal of Molecular Sciences**, v. 22, n. 1, p. 1–17, 2021. <https://doi.org/10.3390/ijms22010427>
- SAMARI, F. *et al* Low-temperature biosynthesis of silver nanoparticles using mango leaf extract: catalytic effect, antioxidant properties, anticancer activity and application for colorimetric sensing. **New Journal of Chemistry**, v. 42, n. 19, p. 15905–15916, 2018. <https://doi.org/10.1039/C8NJ03156H>
- SANTOS, O. A. L. *et al* Environmental Implications Associated with the Development of Nanotechnology: From Synthesis to Disposal. **Nanomaterials**, v. 12, n. 23, p. 4319, 2022. <https://doi: 10.3390/nano12234319>

- SINGH, G.; JALANDHARA, D.; YADAV, K. Effect of grain size on optical properties of iron oxide nanoparticles. **AIP Conference Proceedings**, v. 1728, 2016. <https://doi.org/10.1063/1.4946460>
- SRAVANTHI, K.; AYODHYA, D.; SWAMY, P. Y. Green synthesis, characterization and catalytic activity of 4-nitrophenol reduction and formation of benzimidazoles using bentonite supported zero valent iron nanoparticles. **Materials Science for Energy Technologies**, v. 2, n. 2, p. 298–307, 2019. <https://doi.org/10.1016/j.mset.2019.02.003>
- SRIDEVI, H. *et al* Structural characterization of cuboidal  $\alpha$ -Fe<sub>2</sub>O<sub>3</sub> nanoparticles synthesized by a facile approach. **Applied Nanoscience, Switzerland**, v. 13, n. 8, p. 5605–5613, 2023. <https://doi.org/10.1007/s13204-023-02780-y>
- VINAYAGAM, R. *et al* Structural characterization of marine macroalgae derived silver nanoparticles and their colorimetric sensing of hydrogen peroxide. **Materials Chemistry and Physics**, v. 313, n. September 2023, p. 128787, 2024. <https://doi.org/10.1016/j.matchemphys.2023.128787>
- WUNDER, S. *et al*. Kinetic analysis of catalytic reduction of 4-nitrophenol by metallic nanoparticles immobilized in spherical polyelectrolyte brushes. **Journal of Physical Chemistry C**, v. 114, n. 19, p. 8814–8820, 2010. <https://doi.org/10.1021/jp101125j>